



Contents lists available at ScienceDirect

NDT&amp;E International

journal homepage: [www.elsevier.com/locate/ndteint](http://www.elsevier.com/locate/ndteint)

## Statistical pattern analysis of ultrasonic signals for fatigue damage detection in mechanical structures<sup>☆</sup>

Shalabh Gupta, Dheeraj S. Singh, Asok Ray<sup>\*</sup>

Department of Mechanical Engineering, Pennsylvania State University, University Park, PA 16802, USA

### ARTICLE INFO

#### Article history:

Received 13 December 2007

Received in revised form

17 March 2008

Accepted 2 June 2008

Available online 6 June 2008

#### Keywords:

Fatigue damage monitoring

Ultrasonic sensing methodology

Pattern identification

### ABSTRACT

This paper addresses online monitoring of fatigue damage in polycrystalline alloy structures based on statistical pattern analysis of ultrasonic sensor signals. The real-time data-driven method for fatigue damage monitoring is based on the concepts derived from *statistical mechanics*, *symbolic dynamics* and *statistical pattern identification*. The underlying concept is detection and identification of small changes in statistical patterns of ultrasonic data streams due to gradual evolution of anomalies (i.e., deviations from the nominal behavior) in material structures. The statistical patterns in terms of the escort distributions from statistical mechanics are derived from symbol sequences that, in turn, are generated from ultrasonic sensors installed on the structures under stress cycles. The resulting information of evolving fatigue damage would provide early warnings of forthcoming failures, possibly, due to widespread crack propagation. The damage monitoring method has been validated by laboratory experimentation in real time on a computer-controlled fatigue damage testing apparatus which is equipped with a variety of measuring instruments including an optical travelling microscope and an ultrasonic flaw detector.

© 2008 Published by Elsevier Ltd.

### 1. Introduction

Damage due to fatigue phenomena in polycrystalline alloys is one of the most commonly encountered sources of structural degradation in human-engineered complex electromechanical systems (e.g., aircraft, electric power generation units, and petrochemical plants). Accumulation of fatigue damage may cause catastrophic failures, leading to potential loss of life and expensive equipment. Therefore, it is necessary to develop capabilities for online detection of incipient fatigue damage to ensure safety and reliable operation of human-engineered complex systems as well as for enhancement of their service life. In the current state of the art, direct observation of fatigue damage at an early stage (e.g., crack initiation) is not feasible due to lack of adequate analytical models and sensing devices. Several model-based approaches have been proposed for structural health monitoring and life prediction of mechanical structures [1,2]. Apparently no existing model, solely based on the fundamental principles of material physics, can adequately capture the

dynamical behavior of fatigue damage at the grain level. Specifically, random distribution of flaws in the material microstructure leads to different behavioral trend of fatigue damage evolution in identically manufactured structural components. Consequently, both theoretical and experimental analysis of time series data [3,4] from the available sensors is essential for real-time monitoring of fatigue damage evolution in polycrystalline alloys.

A variety of damage detection techniques, based on different sensing devices (e.g., ultrasonics, acoustic emission, and eddy currents), have been proposed in recent literature for fatigue damage monitoring [5,6]. Acoustic emission technique has been investigated by several researchers for its sensitivity to the activities occurring inside the material microstructure for early detection of fatigue and fracture failures [7,8]. However, the major drawback of acoustic emission technique is poor performance in noisy environments where signal-noise separation becomes a difficult task. The eddy current technique is based on the principal of electromagnetic induction. When a source of alternating current is supplied to a conductor, a magnetic field develops which induces eddy currents in the material. The presence of faults in the material affect the eddy current flow patterns, which can be measured for detection of structural damage [6,9]. The advantages of eddy current inspection technique include sensitivity to small defects, portability of sensor equipment, minimum part preparation, and non-contact evaluation. However, the

<sup>☆</sup> This work has been supported in part by the US Army Research Laboratory and the US Army Research Office under Grant no. W911NF-07-1-0376 and by NASA under Cooperative Agreement no. NNX07AK49A.

<sup>\*</sup> Corresponding author.

E-mail addresses: [szg107@psu.edu](mailto:szg107@psu.edu) (S. Gupta), [dss240@psu.edu](mailto:dss240@psu.edu) (D.S. Singh), [axr2@psu.edu](mailto:axr2@psu.edu) (A. Ray).

limitations of the eddy current inspection technique are the depth of penetration and it can be used to detect only surface and near surface defects. Furthermore, only conductive materials can be inspected.

Ultrasonic sensing technique functions by emitting high frequency ultrasonic pulses that travel through the specimen and are received by the transducers at the other end. As with the propagation of any wave, it is possible that discontinuities in the propagation media will cause additive and destructive interference. Since material characteristics (e.g., voids, dislocations and short cracks) influence the ultrasonic impedance, a small fault in the specimen is likely to change the signature of the signal at the receiver end [10–13]. Specifically, ultrasonic impedance is very sensitive to small microstructural changes occurring during early stages of fatigue damage evolution. Therefore, it is logical to detect the incipient damage from changes in statistical patterns of ultrasonic data due to gradual evolution of anomalies (i.e., deviations from the nominal behavior) in material microstructures. Ultrasonic sensing is suitable for real-time applications and on site installation of the sensing probes is very simple. Ultrasonic sensing technique is also robust to noisy environments since the externally excited waves are of very high frequency and they do not interfere with small disturbances.

The above discussions evince the fact that time series analysis of ultrasonic data is essential for real-time detection and monitoring of fatigue damage. However, appropriate signal processing and pattern identification methods must be incorporated for extraction of relevant information from the ultrasonic time series data. Although there exist diverse techniques of pattern identification [14], only very few of these tools (e.g., artificial neural networks, and principal component analysis) have been applied for online damage detection. Moreover, such applications are largely restricted to the crack propagation regime after a substantial part of the useful service life has already been expended.

This paper presents a novel multidisciplinary approach of pattern identification through integration of the concepts derived from *statistical mechanics* and *symbolic dynamics*. The statistical patterns are identified from observed time series data of sensors for detection of small changes in the underlying process characteristics. The algorithms based on the proposed concept are applied to ultrasonic data for real-time fatigue damage monitoring in polycrystalline alloys. The ultrasonic signals are converted from the time domain to quasi-stationary symbolic sequences by symbolic dynamic encoding [15] using a recently reported statistical pattern identification tool, called symbolic dynamic filtering (SDF) [16]. This procedure enables noise suppression due to symbolization by coarse graining [17], extraction of relevant information by *maximum entropy partitioning* and information compression into low-dimensional probability vectors. Subsequently, behavioral patterns are derived from these probability vectors using escort distributions [18] that are also known as generalized canonical distributions in the statistical physics literature [19].

The escort distributions have the advantage that they are capable of scanning the original probability distribution for increasing the sensitivity of anomaly detection without any significant increase in the computational requirement. Fault signatures are usually hidden in a few elements of the original probability vector (i.e., information is carried by a few symbols) and therefore, the use of escort distribution provides the capability of zooming into certain regions of the partition that reveal more information about the microscopic anomaly progression. As anomalies gradually progress in cyclically stressed structures, the escort distributions evolve relative to the nominal condition and thereby facilitate early detection of small changes in the material microstructure.

The pattern identification algorithms are executable on commercially available inexpensive platforms, thereby allowing real-time implementation. A combination of time series data symbolization and low-dimensional escort pattern generation enables information compression and robust anomaly detection in real time with enhanced sensitivity, especially at early stages of fatigue damage. From the above perspectives, the major contributions of this paper are delineated below:

- (1) Development of a data-driven pattern identification algorithm for real-time fatigue damage monitoring based on the statistical mechanical concept of escort distributions and symbolic dynamic filtering (SDF) of ultrasonic sensor signals.
- (2) Application of the above damage monitoring method for detection of small changes in the material microstructures, especially at early stages of fatigue damage evolution (e.g., crack initiation).
- (3) Experimental validation of the proposed concept on a special-purpose computer-controlled fatigue damage testing apparatus that is equipped with a variety of measuring instruments including an optical traveling microscope and arrays of ultrasonic flaw detectors.

The paper is organized in five sections including the present one. Section 2 outlines the concept of statistical pattern identification using tools of symbolic dynamics and statistical mechanics. Section 3 describes the experimental apparatus on which the proposed concept is validated for early detection of fatigue damage. Section 4 presents the results and discussion and the paper is concluded in Section 5 along with recommendations for future research.

## 2. Problem formulation for behavioral pattern identification

This section presents the behavioral pattern identification problem for anomaly detection in complex dynamical systems. Specifically, the theory of SDF is presented and the concept of escort distributions in statistical mechanics is described for pattern identification and detection of fatigue damage evolution in polycrystalline alloys.

The study of dynamical systems using the tools of statistical mechanics has been a subject of immense interest over the last few decades and is known as *thermodynamic formalism* of complex systems [17,18]. As discussed earlier, detailed models of complex physical processes often prove to be mathematically untractable and computationally intensive especially in the high dimensional phase space. In statistical mechanics, similar issues are dealt with by estimating the macroscopic properties (e.g., pressure, temperature, and chemical potential) of the entire system from the distribution of the elementary particles in various microstates [19]. Following this concept, the behavior of a dynamical system is investigated from both *microscopic* and *macroscopic* perspectives. From the point of view of statistical mechanics, a dynamical system is conceptually visualized to be analogous to a thermodynamic system, where each data point in a sequence of time series data can be treated as a particle in the statistical mechanical sense. The macroscopic behavior of the dynamical system is estimated from the time series data sequences by describing statistical distributions of the (so-called) data particles at different energy levels that are defined by partitioning the time series data sequence as explained in Section 2.1.

Pattern identification of a quasi-stationary process is recognized as a two-time-scale problem. The *fast-time scale* refers to the local behavior of the dynamical system and is defined as the time scale over which the behavior of system dynamics is assumed to

remain invariant (i.e., the process is assumed to have stationary dynamics). From the perspectives of statistical mechanics, the dynamical system remains in quasi-static equilibrium on the same energy hyper-surface in its phase space. In other words, even though, individual particles migrate from one microstate to the other, the probability densities and hence, the macroscopic properties, characteristic of that particular system behavior remain constant over the fast time scale. On the other hand, the *slow-time scale* refers to the long-term behavior of the system, where the patterns of the process dynamics might deviate from those under the nominal condition. It is assumed that any observable non-stationary behavior pattern is associated with changes occurring on the slow time scale. In statistical mechanical analogy, the dynamical system may quasi-statically traverse a path from one energy hyper-surface to another in between two slow time epochs.

In general, a long time span in the fast time scale is a tiny (i.e., several orders of magnitude smaller) interval in the slow time scale. For e.g., evolution of fatigue damage in structural materials (causing a detectable change in the dynamics of the system) occurs on the slow time scale (possibly in the order of months); fatigue damage behavior is essentially invariant on the fast time scale (approximately in the order of seconds or minutes). Nevertheless, the notion of fast and slow time scales is dependent on the specific application and operating environment. As such, for anomaly detection time series data sets are generated on the fast time scale at different slow time epochs.

### 2.1. A brief review of SDF

This section reviews the underlying concepts and essential features of SDF for anomaly detection in dynamical systems [16]. A comparative evaluation of this novel analytical method has shown its superior performance relative to other existing pattern recognition tools in terms of early detection of anomalies [20–22] and robustness to noisy environments [23]. While the details are reported in previous publications [16,23,24], a brief review of the essential concepts of space partitioning and symbol sequence generation is presented here for self-sufficiency, clarity and completeness of the paper. A data sequence is converted to a symbol sequence by partitioning a compact region of the phase space of the dynamical system, over which the trajectory evolves, into finitely many discrete blocks. Each block is labeled as a symbol, where the symbol set  $\Sigma$  is called the *alphabet* that consists of  $|\Sigma|$  different symbols. As the dynamical system evolves in time, it travels through or touches various blocks in its phase space and the corresponding symbol  $\sigma \in \Sigma$  is assigned to it, thus converting the data sequence into a symbol sequence, as shown in Fig. 1. Each symbol is analogous to an energy state in the statistical mechanical sense and therefore the symbols in the alphabet  $\Sigma$  are referred to as states in the sequel. (Note:  $|\Sigma| \geq 2$ , i.e., there are at least two states in this statistical mechanical representation.)

A crucial step in SDF is partitioning of the phase space for symbol sequence generation. Several partitioning techniques have been reported in literature for symbol generation [25], primarily based on symbolic false neighbors. These techniques rely on partitioning the phase space and may become cumbersome and extremely computation intensive if the dimension of the phase space is large. Therefore, as an alternative, symbol sequences can be generated from the measured time series data of available sensors. Fig. 2 presents an illustrative example of partitioning the time series data for symbol sequence generation at a given slow time epoch. Since wavelet transform [26] is particularly effective for noise filtering, the time series data can be pre-conditioned using the wavelet transform [23]. The paper has adopted a partitioning scheme that is called the *maximum entropy*

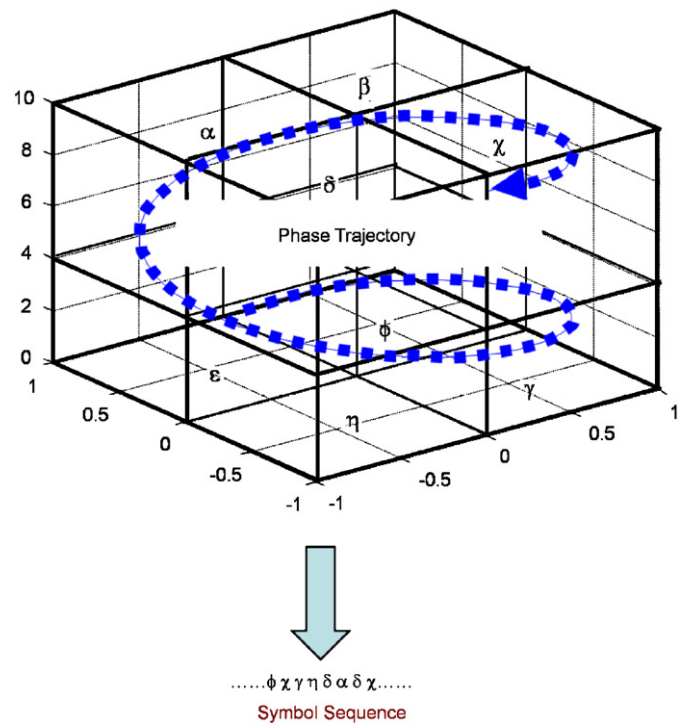


Fig. 1. Concept of phase space partitioning for symbol sequence generation.

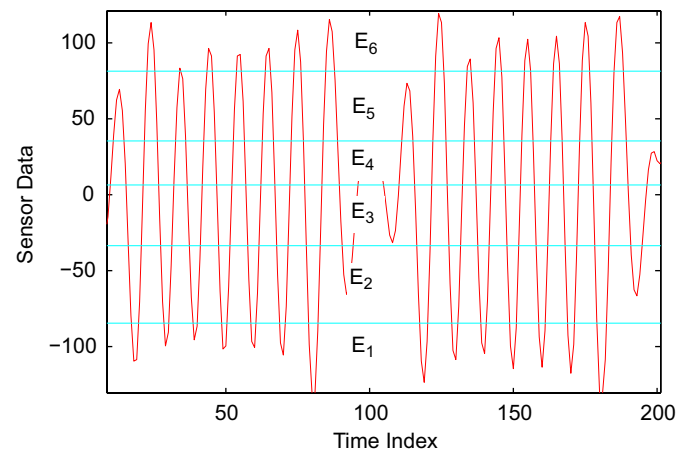


Fig. 2. Illustration of data partitioning for symbol sequence generation.

*partitioning* [16,23]. In this method, the regions with more information are partitioned finer and those with sparse information are partitioned coarser. This is achieved by maximizing the Shannon entropy [27], which is defined as

$$S = - \sum_{i=1}^{|\Sigma|} p_i \log(p_i) \quad (1)$$

where  $p_i$  is the probability of the  $i$ th state and summation is taken over all possible states. Each partition region is identified as an energy state (i.e., a symbol of the alphabet  $\Sigma$ ) in the statistical mechanical sense, as illustrated in Fig. 2. Under the nominal operating condition, uniform probability distribution of energy states, i.e.,  $p_i = 1/|\Sigma|$  for  $i = 1, 2, \dots, |\Sigma|$ , is a consequence of maximum entropy that makes the partition coarser in regions of low data density and finer in regions of high data density [23]. This implies that, under the nominal condition, all energy states are equally likely and have maximum entropy in the statistical

mechanical sense. However, this uniform distribution changes to some other distribution as the dynamical system undergoes degradation, due to growth of anomalies on the slow time epoch.

Once the partitioning is done with alphabet size  $|\Sigma|$  at the nominal condition (i.e., the slow time epoch  $t_0$ ), it is kept constant for subsequent slow time epochs  $\{t_1, t_2, \dots, t_k, \dots\}$ . In essence, the structure of the partition is invariant from the nominal condition. The quasi-stationary probability of transitions from state  $i$  to state  $j$  is denoted as  $\pi_{ij}$ . Thus, stochastic matrix (i.e., each row summing to unity)  $\Pi \equiv [\pi_{ij}]$  describes all transition probabilities between the energy states. Although the algebraic structure of the matrix  $\Pi$  is invariant, the matrix elements may change at different slow time epochs possibly due to gradually evolving anomalies. For quasi-static equilibrium at each epoch,  $\Pi$  is an irreducible stochastic matrix having exactly one eigenvalue equal to unity [28]. The left eigenvector  $\mathbf{p}$  corresponding to the unity eigenvalue of  $\Pi$  is the state probability vector under the (fast time scale) quasi-stationary condition of the dynamical system [16].

The symbol sequence generated from time series data set under the nominal condition, i.e., at time epoch  $t_0$ , is set as the reference point. The *state transition matrix*  $\Pi^0$  at the nominal condition is generated to obtain the *state probability vector*  $\mathbf{p}^0$ , i.e., the left eigenvector of  $\Pi^0$  corresponding to the (unique) unity eigenvalue, whose elements are the stationary probabilities of the energy states. (Note: the superscript indicates the slow time epoch.) Subsequently, state probability vectors  $\mathbf{p}^1, \mathbf{p}^2, \dots, \mathbf{p}^k, \dots$  are obtained at slow-time epochs  $t_1, t_2, \dots, t_k, \dots$  based on the symbol sequences generated from the respective time series data sets.

## 2.2. Escort distributions for pattern identification

As described in the previous subsection, the uniform distribution of the energy states is obtained at the nominal condition as a consequence of maximum entropy partitioning. This represents an internal equilibrium condition of the system under no constraint where all energy states are equally likely. However, this uniform distribution changes to some other distribution as the dynamical system undergoes degradation on the slow time epoch. This means that the system undergoes a transition from the nominal equilibrium condition to another equilibrium condition at a slow time epoch under a constraint that is induced by the growth of anomalies. Therefore, under this changed equilibrium condition, all states are not equally likely and the probability distribution exhibits a deviation from the nominal behavior. This subsection presents the concept of equilibrium distribution as derived from statistical mechanics and its application in dynamical systems theory for pattern identification.

In statistical mechanics, the equilibrium probability distribution of the energy states, called the *generalized canonical distribution*, is estimated by maximizing the entropy of the system for a given macroscopic parameter, such as the energy [18]. This distribution is obtained using the method of *unbiased guess* of the probabilities for a given value of the macroscopic parameter. Let  $E$  be a random variable which takes a value  $E_j$  in the energy state  $j$  and let  $P_j \in \mathbf{P}$  be the equilibrium probability of that state (see Fig. 2). The objective is to estimate the equilibrium probability vector  $\mathbf{P}$  given a macroscopic parameter, such as the total average energy  $\langle E \rangle$ , with the following constraints:

$$\langle E \rangle = \sum_{j=1}^{|\Sigma|} P_j E_j \quad (2)$$

and

$$\sum_{j=1}^{|\Sigma|} P_j = 1. \quad (3)$$

This implies that the equilibrium distribution  $\mathbf{P}$  must satisfy Eq. (2) such that the total average energy of the system is  $\langle E \rangle$ . Eq. (3) is the necessary condition of a probability distribution. In order to obtain the equilibrium distribution, the method of Lagrange multipliers is used [18] for maximization of the entropy function  $S = -\sum_{j=1}^{|\Sigma|} P_j \ln(P_j)$  while the constraints given by Eqs. (2) and (3) are satisfied. Therefore, for infinitesimal variations  $\delta P_j$ , that satisfy Eqs. (2) and (3) in the following form:

$$\sum_{j=1}^{|\Sigma|} E_j \delta P_j = 0, \quad (4)$$

$$\sum_{j=1}^{|\Sigma|} \delta P_j = 0 \quad (5)$$

it is required to have

$$\sum_{j=1}^{|\Sigma|} (1 + \ln(P_j)) \delta P_j = 0 \quad (6)$$

for entropy maximization. Therefore, using the Lagrange method we get from Eqs. (4)–(6)

$$\sum_{j=1}^{|\Sigma|} (\ln P_j - \Psi + \beta E_j) \delta P_j = 0, \quad (7)$$

where  $-\Psi$  and  $\beta$  are the Lagrange multipliers. Since  $\delta P_j$ 's are arbitrary each of the terms in the summation in Eq. (7) must be zero [18]. Therefore, the equilibrium probability distribution, i.e., the *generalized canonical distribution* [18], is obtained from Eq. (7) as follows:

$$P_j = \exp(\Psi - \beta E_j), \quad j = 1, \dots, |\Sigma|. \quad (8)$$

Using Eq. (3),

$$P_j = \frac{\exp(-\beta E_j)}{\sum_{i=1}^{|\Sigma|} \exp(-\beta E_i)}, \quad j = 1, \dots, |\Sigma|, \quad (9)$$

where the parameter  $\beta$  is identified as the inverse of the temperature of the system and  $\exp(-\Psi) = Z(\beta)$  is defined as the partition function that appears as the normalizing factor in Eq. (9), given by the relation

$$Z(\beta) = \sum_{i=1}^{|\Sigma|} \exp(-\beta E_i). \quad (10)$$

As described earlier in Section 2.1, the sensor time series data is partitioned to generate the symbol sequences and the state probabilities are obtained for each energy state as described by the probability vector  $\mathbf{p}$ . The objective now is to assign the equilibrium distribution, i.e., the generalized canonical distribution (using Eq. (9)), to the energy states, as shown in Fig. 2. This is achieved by relating the statistical mechanical concepts using the equilibrium distribution as described above to the original state probability vector  $\mathbf{p}$ . For dynamical systems, using the *thermodynamic formalism* as shown in Ref. [18], the energy states  $E_j$ 's are related to the state probabilities  $p_j$ 's by the following relation:

$$E_j = -\ln p_j, \quad j = 1, \dots, |\Sigma|, \quad (11)$$

where  $p_j$  is observed probability (obtained from partitioning the experimental data using SDF as described in Section 2.1) of the  $j$ th energy state. The rationale for the above substitution are given below:

- Since  $-\ln p_j \geq 0$ , this implies  $0 \leq E_j \leq \infty$ .
- The partition levels that have low frequency of visit (i.e., regions with low information content) have corresponding high energies (less reachable) and the partition levels that have

high frequency of visit (i.e., regions with high information content) have corresponding low energies (more reachable) in the statistical mechanical sense. E.g., if state  $j$  is never visited, i.e.,  $p_j = 0$ , then it corresponds to infinite energy state that is never reached by a particle.

Using Eq. (11) in Eq. (9) we get,

$$P_j = \frac{(p_j)^\beta}{\sum_{j=1}^{|\Sigma|} (p_j)^\beta}, \quad j = 1, \dots, |\Sigma| \quad (12)$$

which provides the generalized canonical distribution  $\mathbf{P}$ , also called as the *escort distribution* of  $\mathbf{p}$  of order  $\beta$ . The escort distribution  $\mathbf{P}$  has the ability to scan the structure of the original probability distribution  $\mathbf{p}$ . The order  $\beta$  that is analogous to inverse temperature in the statistical mechanical sense, affects the relative importance of how the microstates  $j$  enter into the escort distribution. Therefore, the escort distribution  $\mathbf{P}$  reveals more information of the system than the original probability distribution  $\mathbf{p}$ . Note that the escort distribution  $\mathbf{P}$  is equal to the original probability distribution  $\mathbf{p}$  at the nominal condition (i.e., uniform distribution at time epoch  $t_0$ ) irrespective of  $\beta$ , such that

$$P_j^0 = p_j^0 = 1/|\Sigma|, \quad j = 1, \dots, |\Sigma|. \quad (13)$$

Since  $\beta \sim 1/T$ , where  $T$  is the effective temperature, evaluation of the probability distribution  $\mathbf{p}$  at different values of  $\beta$  (see Eq. (12)) is interpreted as analogous to a change of temperature in a thermodynamic system [18]. This statistical mechanical analogy of temperature does not represent the true temperature of the stressed structure and only serves as a dynamical system parameter for sensitivity analysis.

When  $\beta \rightarrow 0$ , the temperature  $T$  tends to  $\infty$  in the statistical mechanical sense, which means that the system becomes random and the uncertainty in the system becomes very high such that all the energy states become equally excited. This leads to equal escort probability ( $P_j = 1/|\Sigma|, j = 1, \dots, |\Sigma|$ ) of each energy state and due to the maximum uncertainty, the information content obtained from the system is minimized. The escort distribution  $\mathbf{P}$  approaches the uniform distribution at any anomalous condition for  $\beta \rightarrow 0$ ; this is different from the nominal condition in Eq. (13), where  $\mathbf{P}$  is the uniform distribution irrespective of  $\beta$  because the original distribution  $\mathbf{p}$  is itself uniform as a consequence of maximum entropy partitioning [23] (see Section 2.1). On the other hand as  $\beta \rightarrow \infty$ , the escort distribution approaches the dirac-delta distribution in the lowest energy state and the system freezes to no activity. As seen in Eq. (11), the value of this lowest possible energy state is zero whose probability is one. In between these two extreme cases, as the value of  $\beta$  is increased from zero (i.e., the temperature  $T$  is decreased), the uncertainty is reduced and more information is revealed. Therefore, at a higher  $\beta$  (i.e., a lower temperature  $T$ ), many new facets of the system are revealed. As  $\beta$  is increased, the higher (lower) probability states become more (less) dominant and vice versa. Therefore, the escort distribution with a higher  $\beta$  yields a better revelation of the system information during early stages of fatigue damage evolution and is capable of providing early warnings of catastrophic failure, which can be used for appropriate control action. Further details are provided in Section 4.

The major advantages of the pattern identification method presented in this paper for anomaly detection are listed below:

- (a) Robustness to measurement noise and spurious signals due to coarse graining of the continuous data (i.e., partitioning into finite blocks) and generation of a symbol sequence that eliminates small measurement noise [16,23].

- (b) Adaptability to low-resolution sensing due to coarse graining in space partitions [16].
- (c) Capability for early detection of anomalies because of enhanced sensitivity to signal distortion using escort distributions.
- (d) Real-time execution on commercially available inexpensive platforms [20,21].

### 2.3. Damage evolution and anomaly detection

The pattern changes are quantified as deviations from the nominal behavior (i.e., the escort distribution at the nominal condition). The resulting anomalies (i.e., deviations of the evolving patterns from the nominal pattern) are characterized by a scalar-valued function, called *anomaly measure*  $\psi$  that is quasi-static in the fast time scale and is monotonically non-decreasing in the slow time scale. The escort probability vector at any time epoch corresponds to a singleton point on the unity-radius hypersphere. During fatigue damage evolution, the tip of the escort probability vector moves along a path on the surface of this hypersphere. The initial starting point of the path is the escort probability vector  $\mathbf{P}^0$  with uniform distribution obtained with maximum entropy partitioning [23]. As the damage progresses, the escort distribution (for a non-zero, finite and constant value of order  $\beta$ ) changes; eventually when a very large crack is formed, complete attenuation of the ultrasonic time series data occurs (see Section 3). Consequently the tip of the escort probability vector reaches a point where all states have zero probabilities of occurrence except one which has a probability one (i.e., a delta distribution  $\mathbf{P}^f$ ); this state corresponds to the partition region where all data points are clustered due to complete attenuation of the signal. In the context of an irreversible process such as fatigue crack growth phenomena, the anomaly measure is based on the following assumptions:

- *Assumption #1:* The damage evolution is an irreversible process (i.e., with zero probability of self healing) and implies the following conditions:

$$\psi(t) \geq 0; \quad \psi(t + \delta) - \psi(t) \geq 0 \quad \forall t \geq t_0 \quad \forall \delta > 0. \quad (14)$$

- *Assumption #2:* The damage accumulation between two time epochs is a path function, i.e., dependent on the path traversed to reach the target state from the initial state.

At the initial stages of fatigue damage, there can be multiple short cracks oriented in different directions. Therefore, crack length alone does not provide complete information on fatigue damage evolution. Since ultrasonic signals are highly sensitive to small microstructural changes, signal distortion is a good index of anomaly growth. As such, the following distance function is used between the escort probability vectors at two time epochs:

$$d(\mathbf{P}^k, \mathbf{P}^l) \equiv \sqrt{(\mathbf{P}^k - \mathbf{P}^l)^T (\mathbf{P}^k - \mathbf{P}^l)}. \quad (15)$$

The escort probability vector depends on the distribution  $\mathbf{p}$ , which might be affected by measurement and computation noise. The algorithm for computation of the anomaly measure  $\psi$  compensates for spurious measurement and computation noise in terms of the sup norm  $\|\mathbf{e}\|_\infty \equiv \max(|e_1|, \dots, |e_m|)$  of the error in the state probability vector (i.e., the maximum error in the elements of the state probability vector  $\mathbf{p}$ ). The algorithm is presented below:

- (i)  $\psi^0 = 0, \delta\psi^1 = 0, \tilde{\mathbf{P}} = \mathbf{P}^0, \tilde{\mathbf{p}} = \mathbf{p}^0$ , and  $k = 1$ .
- (ii) if  $\|\mathbf{p}^k - \tilde{\mathbf{p}}\|_\infty > \varepsilon$  then  $\delta\psi^k = d(\mathbf{P}^k, \tilde{\mathbf{P}}), \tilde{\mathbf{p}} \leftarrow \mathbf{p}^k$ , and  $\tilde{\mathbf{P}} \leftarrow \mathbf{P}^k$ .

- (iii)  $\psi^k = \psi^{k-1} + \delta\psi^k$ , and  $k \leftarrow k + 1$ .
- (iv)  $\delta\psi^k = 0$ ; go to step (ii),

where the real positive parameter  $\varepsilon$ , associated with robustness of the anomaly measure for measurement and computation noise, is identified by performing an experiment with a sample with no notch (see Section 3). Since there is no notch, there is practically no stress augmentation and relatively no fatigue damage, and the parameter  $\varepsilon$  is estimated as

$$\varepsilon \approx \max_{l \in \{1, \dots, N\}} (\|\mathbf{p}^{l+1} - \mathbf{p}^l\|_\infty) \quad (16)$$

from  $N$  consecutive observations with  $N \gg 1$ . The algorithm works in the following way.

The reference point  $\tilde{\mathbf{P}}$  is initialized to be the nominal escort distribution  $\mathbf{P}^0$  and  $\tilde{\mathbf{p}}$  is initialized to be the nominal state probability vector  $\mathbf{p}^0$ , and the anomaly measure  $\psi^0$  is set to 0. At any subsequent slow time epoch  $t_k$ , if the state probability vector moves such that the distance moved in any particular direction (i.e., the sup norm  $\|\bullet\|_\infty$ ) is greater than  $\varepsilon$  as specified in step (ii), then the anomaly measure is incremented by  $\delta\psi^k = d(\mathbf{P}^k, \tilde{\mathbf{P}})$  and the reference points are shifted to the current points  $\mathbf{P}^k$  and  $\mathbf{p}^k$ . The procedure is repeated at all slow time epochs. As such, the total path travelled by the tip of the escort probability vector represents the associated damage.

#### 2.4. Summary of the steps followed

1. Time series data acquisition from appropriate sensor(s) (here ultrasonic transducers) at time epoch  $t_0$ , i.e., the nominal condition, when the system is assumed to be in the healthy state (i.e., zero anomaly measure).
2. Generation of the *maximum entropy partition* based on the nominal time series data set after signal conditioning for noise removal using wavelets [23]. The partitioning is fixed for subsequent time epochs  $t_1, t_2, \dots, t_k, \dots$
3. Calculation of the state probability vector  $\mathbf{p}^0$  (see Section 2.1) and the corresponding escort probability vector  $\mathbf{P}^0$  for a certain order parameter  $\beta$  (see Section 2.2) at time epoch  $t_0$ .  $\mathbf{P}^0$  is a uniform distribution because of maximum entropy partitioning [23].
4. Collection of ultrasonic time series data sets at slow time epochs  $t_1, t_2, \dots, t_k, \dots$  and calculation of the corresponding escort probability vectors  $\mathbf{P}^1, \mathbf{P}^2, \dots, \mathbf{P}^k, \dots$
5. Computation of the scalar *anomaly measures*  $\psi^1, \psi^2, \dots, \psi^k, \dots$ , at time epochs  $t_1, t_2, \dots, t_k, \dots$  (see Section 2.3).

### 3. Description of the experimental apparatus

The experimental apparatus, shown in Fig. 3, is a special-purpose uniaxial fatigue testing machine, which is operated under load control or strain control at speeds up to 12.5 Hz; a detailed description of the apparatus and its design specifications are reported in [29]. The test specimens are subjected to tensile-tensile cyclic loading by a hydraulic cylinder under the regulation of computer-controlled electro-hydraulic servo-valves. The damage detection subsystem consists of data analysis software and the associated computer hardware.

#### 3.1. Instrumentation and control system

The process instrumentation and the control module of the fatigue test apparatus are briefly described below:

- *Closed loop servo-gydraulic unit and controller*: The instrumentation and control of the computer-controlled uniaxial fatigue test

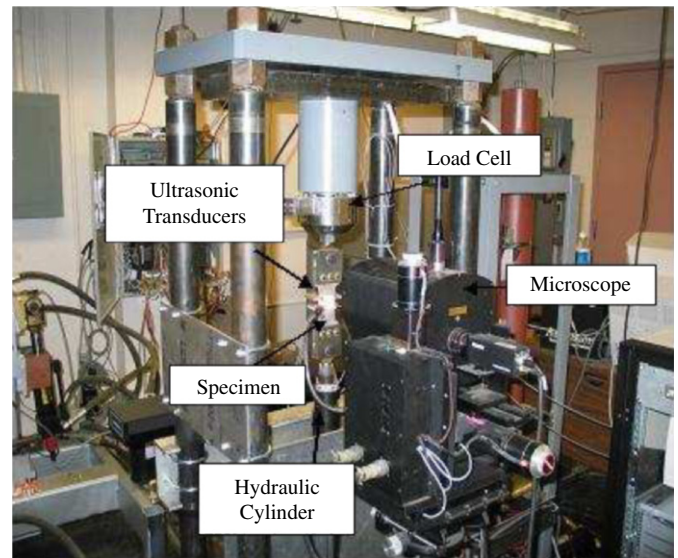


Fig. 3. Special-purpose fatigue test apparatus.

apparatus includes a load cell, an actuator, the hydraulic system, and the controller. The servo-hydraulic unit can provide either random loads or random strains to a specimen for both low-cycle and high-cycle fatigue tests at variable amplitudes and multiple frequencies. The control module is installed on a computer which is dedicated to machine operation. The controller runs the machine according to a schedule file which contains the loading profile and the number of load cycles. The real-time data from the extensometer and load cell are supplied to the controller for operation under specified position and load limits.

- *Subsystem for data acquisition, signal processing, and engineering analysis*: In addition to the computer for controlling the load frame, a second computer is used for real-time image data collection from the microscope to monitor the growth of surface cracks. This computer controls the movement of the microscope to focus on the region of the crack tip. The instrumentation for ultrasonic flaw detection scheme is connected to a third computer. This computer performs the real-time data analysis task. These laboratory computers are interconnected by a local dedicated network for data acquisition, data communications, and control.

Fig. 4 shows a typical 7075-T6 side notched aluminum specimen used for testing in the fatigue damage test apparatus. The specimens used are 3 mm thick and 50 mm wide, and have a slot of 1.58 mm × 4.57 mm on one side. The notch is made to increase the stress concentration factor that ensures crack initiation and propagation at the notch end. The test specimens have been subjected to sinusoidal loading under tension-tension mode (i.e., with a constant positive offset) at a frequency of 12.5 Hz. The DC offset was provided in the load cycling to ensure that the specimen was always under tension. Since inclusions and flaws are randomly distributed across the material, small cracks appear at these defects and propagate and join at the machined surface of the notch even before microscopically visual cracks appear on the surface.

#### 3.2. Sensing system for damage detection

The test apparatus is equipped with two types of sensors that have been primarily used for damage detection:

- (1) *Travelling optical microscope*: The travelling optical microscope, shown as part of the test apparatus in Fig. 3, provides direct

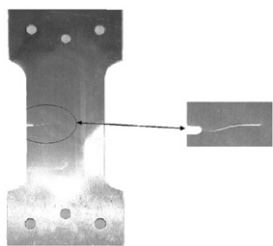


Fig. 4. Cracked specimen with a side notch.

measurements of the visible portion of a crack. The resolution of the optical microscope is about  $2\mu\text{m}$  at a working distance of 10–35 cm and the images are taken at a magnification of  $75\times$ . The growth of the crack is monitored continuously by the microscope which takes the images of the surface of the specimen at regular intervals. In order to take pictures the controller slows down the machine to less than 5 Hz to get a better resolution of the images. The crack length can be calculated automatically by movement of the microscope from the respective notch end to the tip of the crack. The data acquisition software also allows for manual operation and image capture at the desired moment. Formation of very small cracks is difficult to detect and model due to large variability of material irregularities. This paper primarily focuses on analyzing ultrasonic data for more accurate characterization of the nature of small defects.

(2) *Ultrasonic flaw detector*: A piezoelectric transducer is used to inject ultrasonic waves in the specimen and an array of receiver transducers is placed on the other side of notch to measure the transmitted signal. In these experiments, an array of two receiver transducers was placed below the notch to detect faults on both left and right side of the notch. The ultrasonic waves produced were 5 MHz sine wave signals and they were emitted during a very short portion at the peak of every load cycle. Ultrasonic measurements were taken at stress levels that exceeded the crack opening stress and this causes maximum attenuation of the ultrasonic waves. Note that if crack closure occurs at low loads, then an alternative method would be needed to detect anomalies. The sender and receiver ultrasonic transducers are placed on two positions, above and below the notch, so as to send the signal through the region of crack propagation and receive it on the other side, as seen in Fig. 5.

As with the propagation of any wave, it is possible that discontinuities in the propagation media will cause additive and destructive interference. Since material characteristics (e.g., voids, dislocations and short cracks) influence ultrasonic impedance, a small fault in the specimen is likely to change the signature of the signal at the receiver end. The effect of these discontinuities in the material is to distort the transmitting ultrasonic waves. Since ultrasonic waves have a very small wavelength, very small faults can be detected. Therefore, the received signal can be used to capture minute details and small changes during the early stages of fatigue damage, which are not possible to detect by an optical microscope [11]. Prior to the appearance of a single large crack on the surface of the specimen as detected by the optical microscope, deformations (e.g., dislocations and short cracks) can cause detectable attenuation and/or distortion of the ultrasonic waves [12]. Recent literature has also shown nonlinear modeling approaches of the ultrasonic interference with the material microstructures [30,31]. An elaborate description of the properties of ultrasonic waves in solid media is provided by Rose [32].

The advantages of using ultrasonic flaw detection over a microscope are the ease of installation at the desired damage site and detection of early anomalies before the onset of widespread fatigue crack propagation. It is observed that a crack always starts

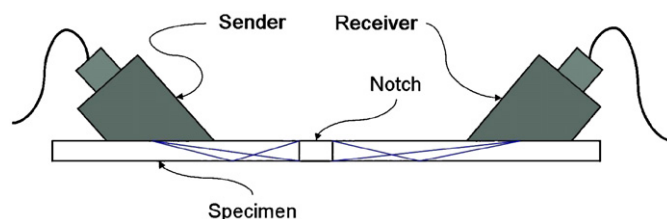


Fig. 5. Ultrasonic flaw detection scheme.

at the stress-concentrated region near the notch but the exact site of crack nucleation can be treated as a random event. An optical microscope is only capable of detecting cracks when they appear on the front surface of the specimen. Therefore, the study in this paper is based on analyzing the ultrasonic data for identification of fatigue damage in the small crack regime.

### 3.3. Experimentation and data acquisition

The optical images were collected automatically at every 200 cycles until a crack was detected on the specimen surface by the optical microscope. Subsequently, the images were taken at user command and the microscope was moved such that it always focused on the crack tip. A significant amount of microstructural damage caused by multiple small cracks, dislocations and other defects occurs before a single large crack appears on the surface of the specimen when it is observed by the optical microscope [33]. This phenomenon causes distortion and attenuation of the ultrasonic signal at the receiver end. The crack propagation stage starts when this microstructural damage eventually develops into a single large crack. Subsequently, the crack growth rate increases rapidly and when the crack is sufficiently large, complete attenuation of the transmitted ultrasonic signal occurs, as seen at the receiver end. After the crack appears on the surface, fatigue damage growth can be easily monitored by the microscope but the ultrasonics provide early warnings even during the crack initiation phase.

Ultrasonic waves with a frequency of 5 MHz were triggered at each peak of the sinusoidal load to generate data points in each cycle. Since the ultrasonic frequency is much higher than the load frequency, data acquisition was done for a very short interval in the time scale of load cycling. Therefore, it can be implied that ultrasonic data were collected at the peak of each sinusoidal load cycle, where the stress is maximum and the crack is open causing maximum attenuation of the ultrasonic waves. The slow time epochs for data analysis were chosen to be 1000 load cycles (i.e.,  $\sim 80\text{ s}$ ) apart. At the onset of each slow time epoch, the ultrasonic data points were collected on the fast time scale of 50 cycles (i.e.,  $\sim 4\text{ s}$  at 12.5 Hz frequency), which produced a string of 30,000 data points. It is assumed that during this period, the system remained in a stationary condition and no major changes occurred in the fatigue crack behavior. The sets of time series data collected in this manner at different slow-time epochs were analyzed to calculate the anomaly measures at those slow time epochs.

The nominal condition at the slow time epoch  $t_0$  was chosen to be  $\sim 1$  kilocycles to ensure that the electro-hydraulic system of the test apparatus had come to a steady state and that no significant damage occurred till that point. This nominal condition was chosen as a benchmark where the specimen was assumed to be in a healthy state, and thus the anomaly measure was chosen to be zero. The anomalies at subsequent slow-time epochs,  $t_1, t_2, \dots, t_k, \dots$ , were then calculated with respect to the nominal condition at  $t_0$ . It is emphasized that the anomaly measure is relative to the nominal condition which is fixed in advance and should not be confused with the actual damage at an absolute

level. However, inferring fatigue damage from the observed anomaly measure is an inverse problem that is a topic of future research.

The fatigue tests were conducted at a constant amplitude sinusoidal load for low-cycle fatigue, where the maximum and minimum loads were kept constant at 87 and 4.85 MPa, respectively. For low cycle fatigue studied in this paper, the stress amplitude at the crack tip is sufficiently high to observe the elasto-plastic behavior in the specimens under cyclic loading. A significant amount of internal damage caused by multiple small cracks, dislocations and microstructural defects alters the ultrasonic impedance, which results in signal distortion and attenuation at the receiver end. The crack propagation stage starts when this internal damage eventually develops into a single large crack.

### 3.4. Real-time implementation

Fatigue damage monitoring algorithms have been successfully implemented in real time. The function module for the pattern identification algorithms is triggered at the start of the experiment after the system obtains the steady state. The ultrasonic data files generated in real time at different slow time epochs are read by the pattern identification algorithms that calculate the anomaly measure values at these time epochs. The algorithm is computationally very fast (i.e., several orders of magnitude faster relative to slow-time-scale damage evolution) and the anomaly measure profile is displayed on a computer monitor in real time. The plot is updated with the most recent value of anomaly measure at each (slow-time) epoch. Thus, the algorithms allows on-line health monitoring and is capable of issuing warnings of incipient failures well in advance. Superiority of the symbolic dynamic method relative to Bayesian methods in terms of execution time and memory requirement is reported by Rao et al. [22].

## 4. Results and discussion

This section presents the results generated from the time series data of ultrasonic sensors for early detection of fatigue damage using the concepts presented in earlier sections. The six triplets of plots in Fig. 6 show two-dimensional images of the specimen surface, the ultrasonic response, and the corresponding escort probability distribution of energy states, with  $|\Sigma| = 6$ , at six different slow time epochs, approximately 1, 10, 18, 23, 32, and 45 kilocycles, exhibiting gradual evolution of fatigue damage. For each time epoch, i.e., each plot in Fig. 6, the escort distribution is shown for different values of  $\beta = 0, 0.5, 1, 2, 5, \text{ and } 10$ . In each of the six plot triplets, the top plot exhibits the image of the test specimen surface near the notch as seen by the optical microscope.

The plot triplet (a) of Fig. 6 shows the image at the nominal condition ( $\sim 1$  kilocycles). The maximum entropy principle used for partitioning has led to a uniform escort probability distribution in the energy states as seen in the histograms for all values of order  $\beta$  as explained earlier in Section 2.2. The anomaly measure at this point is taken to be zero. Plot triplets (b) and (c) at  $\sim 10$  and  $\sim 18$  kilocycles, respectively, do not yet have any indication of surface crack but the escort distribution histograms of different orders  $\beta$  exhibit deviations from the uniform probability distributions in plot triplet (a). This is an evidence that the analytical measurements, based on ultrasonic sensor data, produce damage information during the crack initiation stage. The detection also becomes more distinguished at higher values of order  $\beta$ . The visual inspection of the ultrasonic response seen in plots (b) and

(c) does not reveal much information; however, the escort distributions clearly indicate progression of anomalies.

The image in plot (d) of Fig. 6 at  $\sim 23$  kilocycles exhibits the first noticeable appearance of a small surface crack, this may be considered as the boundary of the crack initiation and the propagation phases. This indicates that a single or possibly several small cracks might have already developed underneath the surface before they merged into a single surface crack. The corresponding histograms in the plot triplet (d) show further deviation from the uniform distribution of plot triplet (a). The image in plot triplet (e) at  $\sim 32$  kilocycles exhibits a fully developed crack in its propagation phase. The corresponding histograms show significant variation from those in earlier stages, from plot triplets (a) to (d). The image in plot triplet (f) at  $\sim 45$  kilocycles exhibits a large crack or a broken specimen. The corresponding histograms resemble a delta distribution indicating complete attenuation of the ultrasonic data.

In all the histogram plots in Fig. 6 at different time epochs, the escort probabilities of all energy states are equal to the uniform distribution for  $\beta = 0$ , irrespective of the system health. This indicates that, for  $\beta = 0$ , i.e.,  $T \rightarrow \infty$ , the system attains a maximum entropy state resulting in no information retrieval. In all plots, as  $\beta$  is increased from  $\beta = 0$ , more information is revealed which is of significant importance especially during the crack initiation when the specimen has just started developing internal cracks with no external manifestation. Therefore, higher order escort distributions yield a better picture of the system with distinct probability distributions. As  $\beta$  is increased, the higher probability states become more significant and lower probability states become less significant resulting in more sensitivity to small change detection. In all plots of Fig. 6, as  $\beta$  is increased from 0 to 10, the difference in escort probabilities of different states become more noticeable.

Fig. 7 shows the profile of anomaly measure representing the evolution of fatigue damage at different slow time epochs. The anomaly measure profiles are plotted for different values of  $\beta = 0, 0.5, 1, 2, 5, \text{ and } 10$  by comparison of escort distribution of like orders using the procedure described in Section 2.3. In the region around  $\sim 20$ – $23$  kilocycles, a rapid change in the slope of anomaly measure profiles is observed for all  $\beta$  that indicates the onset of crack propagation phase. The vertical line in Fig. 7 broadly classifies two regions, one of crack initiation and small crack development (towards the left of the vertical line) and the other of crack propagation where a single large crack grows rapidly (towards the right of the vertical line). Once the crack propagation starts the growth of anomaly measure is very fast till complete breakage of the specimen.

For  $\beta = 0$ , the profile of anomaly measure in Fig. 7 is uniformly zero yielding no information. This is also evident from Fig. 6 where the escort distribution for  $\beta = 0$  remains the uniform distribution for all time epochs as shown in six different plot triplets. For smaller values of  $\beta$  (e.g.,  $0.5$ – $1$ ), the anomaly measure profiles derived from the escort probability distributions effectively capture the crack propagation phase; however, the crack initiation phase is not adequately detected. This is indicated by relatively high values of slope and magnitude of anomaly measure profiles in the crack propagation phase as compared to the crack initiation phase.

That is, for smaller values of  $\beta$ , the anomaly measure profiles are less capable of issuing early warnings for progressive damage in the crack initiation phase. As  $\beta$  is increased, the anomaly measure profile shows a more sensitive response to damage growth, specially in the crack initiation phase in terms of both the magnitude and the slope of the anomaly measure. As  $\beta$  is increased (e.g.,  $\beta > 1$ ), the anomaly measure profile shows relatively large deviations from the nominal condition even

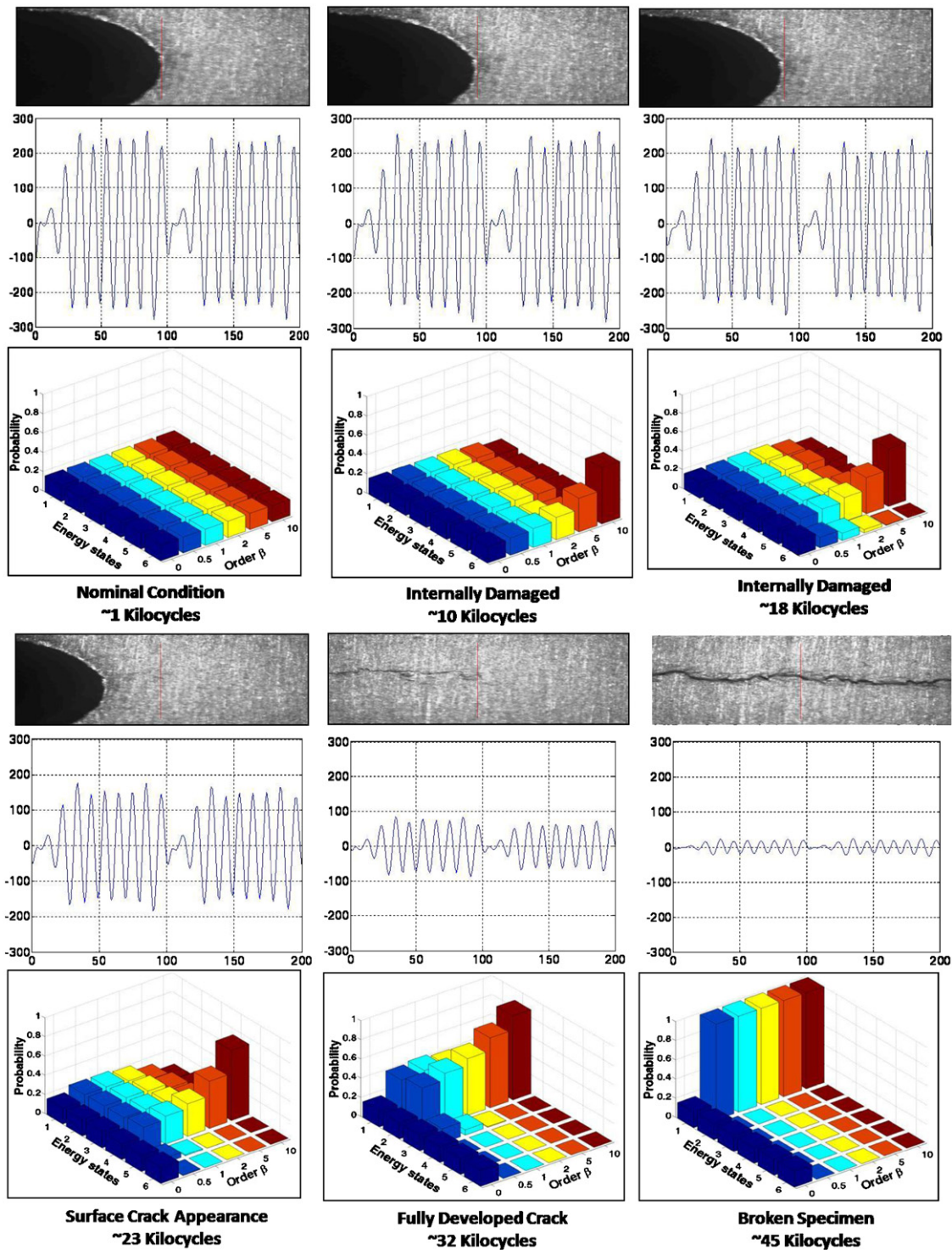


**Fig. 6.** Fatigue damage evolution and corresponding information from escort distributions of different order  $\beta = 0, 0.5, 1, 2, 5$  and  $10$ ; (a) nominal condition at  $\sim 1$  kilocycles, (b) microstructural damaged condition at  $\sim 10$  kilocycles, (c) microstructural damaged condition at  $\sim 18$  kilocycles, (d) appearance of a surface crack at  $\sim 23$  kilocycles, (e) crack propagation condition with fully developed crack at  $\sim 32$  kilocycles, and (f) broken condition at  $\sim 45$  kilocycles.

during the early stages of crack initiation. In the crack propagation phase, the profiles of all  $\beta > 0$  are sensitive in effectively detecting fatigue damage. However, in the crack initiation phase which is primarily the region of interest, the anomaly measure profiles derived from higher order escort distributions play a significant role in early damage detection.

Increasing  $\beta$  to high values (e.g., 5–10) would be advantageous in the initial stages of fatigue damage for early detection. However, increasing  $\beta$  to even higher values (e.g.,  $\beta > 10$ ) would

make the system over-sensitive resulting in a sharp jump in the anomaly measure profile for small changes and may possibly lead to false alarms. A sudden jump in anomaly measure profile for small changes is not desirable from the perspective of continuous monitoring of fatigue damage evolution during the entire span of the service life. As such,  $\beta$  should be optimized for desired sensitivity which is an area of future research.

It is to be noted that anomaly measure for fatigue damage detection is relative to the nominal condition and is not an

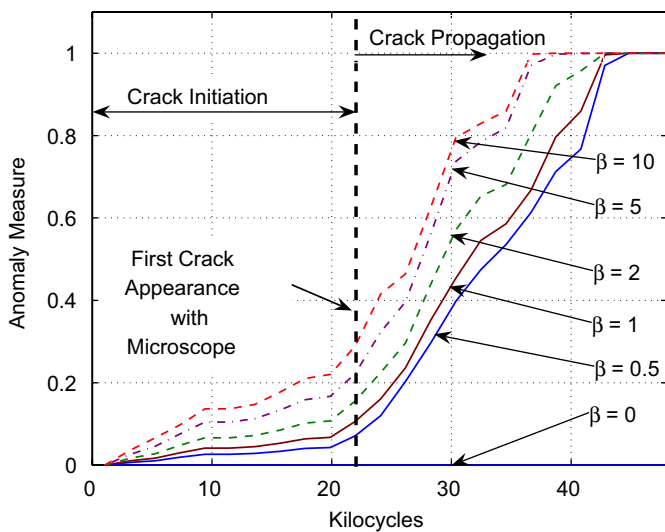


Fig. 7. Anomaly measure profiles for fatigue damage evolution derived from escort distributions of different order  $\beta = 0, 0.5, 1, 2, 5,$  and  $10$ .

indicative of true damage in the absolute sense. Furthermore, due to the presence of several microstructural uncertainties, fatigue damage evolution is considered as a stochastic phenomenon and identical specimen can reveal significantly different damage evolution profiles under similar loading conditions. Therefore, damage quantification is a difficult task and requires statistical analysis of an ensemble of experimental data. In this regard, the problem of fatigue damage monitoring is divided into (i) the forward problem of anomaly detection and (ii) the inverse problem of anomaly quantification. The current paper has attempted to address the forward problem, i.e., the problem of fatigue damage detection by measurement of statistical changes in the ultrasonic data streams relative to the nominal condition. The complete solution of the inverse problem is still an area of active research.

## 5. Conclusions and future work

This paper presents the theory and experimental validation of fatigue damage detection significantly before the onset of wide-spread damage due to rapid crack propagation. The real-time data analysis method makes use of the ultrasonic time series data and is based on the concepts of symbolic dynamic filtering and escort distributions derived from statistical mechanics. Statistical pattern changes in escort distributions of the observed time series data sequences at different slow time epochs capture the gradual evolution of microstructural changes in polycrystalline alloys. The concepts have been experimentally validated on a computer-controlled special-purpose fatigue damage test apparatus.

Further analytical and experimental research is necessary before the proposed methodology of fatigue damage monitoring could be implemented in industrial applications. Specifically, the following research tasks are recommended for future work:

- Comparison with other sensing methods for fatigue damage detection such as the acoustic emission and the eddy current techniques.
- Development of damage mitigation control strategies on the basis of the inferred anomalies from sensor data by time series analysis in real time.
- Development of thermodynamic formalism for time series data analysis using the statistical mechanical tools of lattice spin systems such as the Ising model [19,34].

- Development of statistical methods based on thermodynamic formalism for real-time estimation [35] and prognosis of fatigue damage in polycrystalline alloys.

## References

- [1] Meggiolaro M, Castro J. Statistical evaluation of strain-life fatigue crack initiation predictions. *Int J Fatigue* 2004;26:463–76.
- [2] Ishihara S, McEvily A. Analysis of short fatigue crack growth in cast aluminium alloys. *Int J Fatigue* 2002;24:1169–74.
- [3] Kantz H, Schreiber T. *Nonlinear time series analysis*. 2nd ed. Cambridge, UK: Cambridge University Press; 2004.
- [4] Daw C, Finney C, Tracy E. A review of symbolic analysis of experimental data. *Rev Sci Instrum* 2003;74(2):915–30.
- [5] Grondel S, Delebarre C, Assaad J, Dupuis J, Reithler L. Fatigue crack monitoring of riveted aluminium strap joints by lamb wave analysis and acoustic emission measurement techniques. *NDT&E Int* 2002;35:137–46.
- [6] Zilberstein V, Walrath K, Grundy D, Schlicker D, Goldfine N, Abramovici E, Yentzer T. Mwm eddy-current arrays for crack initiation and growth monitoring. *Int J Fatigue* 2003;25:1147–55.
- [7] Baram J. Fatigue-life prediction by an order statistics treatment of acoustic-emission signals. *Exp Mech* 1993;33:189–94.
- [8] Harris DO, Dunegan HL. Continuous monitoring of fatigue-crack growth by acoustic-emission techniques. *Exp Mech* 1974;14:71–80.
- [9] Zilberstein V, Grundy D, Weiss V, Goldfine N, Abramovici E, Newman J, et al. Early detection and monitoring of fatigue in high strength steels with mwm-arrays. *Int J Fatigue* 2005;27:1644–52.
- [10] Anson L, Chivers R, Puttick K. On the feasibility of detecting pre-cracking fatigue damage in metal matrix composites by ultrasonic techniques. *Compos Sci Technol* 1995;55:63–73.
- [11] Keller E, Ray A. Real time health monitoring of mechanical structures. *Struct Health Monit* 2003;2(3):191–203.
- [12] Rokhlin S, Kim J-Y. In situ ultrasonic monitoring of surface fatigue crack initiation and growth from surface cavity. *Int J Fatigue* 2003;25:41–9.
- [13] Kenderian S, Berndt T, Green R, Djordjevic B. Ultrasonic monitoring of dislocations during fatigue of pearlitic rail steel. *Mater Sci Eng* 2003;348:90–9.
- [14] Duda R, Hart P, Stork D. *Pattern classification*. New York, NY, USA: Wiley; 2001.
- [15] Lind D, Marcus M. *An introduction to symbolic dynamics and coding*. Cambridge, UK: Cambridge University Press; 1995.
- [16] Ray A. Symbolic dynamic analysis of complex systems for anomaly detection. *Signal Process* 2004;84(7):1115–30.
- [17] Badii R, Politi A. *Complexity hierarchical structures and scaling in physics*. Cambridge, UK: Cambridge University Press; 1997.
- [18] Beck C, Schlögl F. *Thermodynamics of chaotic systems: an introduction*. Cambridge, UK: Cambridge University Press; 1993.
- [19] Pathria R. *Statistical mechanics*. Oxford, UK: Butterworth Heinemann; 1996.
- [20] Chin S, Ray A, Rajagopalan V. Symbolic time series analysis for anomaly detection: a comparative evaluation. 2005;85(9):1859–68.
- [21] Gupta S, Ray A, Keller E. Symbolic time series analysis of ultrasonic data for early detection of fatigue damage. *Mech Syst Signal Process* 2007;21(2):866–84.
- [22] Rao C, Ray A, Sarkar S, Yasar M. Review and comparative evaluation of symbolic dynamic filtering for detection of anomaly patterns. *Signal Image Video Process (SIVP)* 2008 DOI:10.1007/s11760-008-0061-8.
- [23] Rajagopalan V, Ray A. Symbolic time series analysis via wavelet-based partitioning. *Signal Process* 2006;86(11):3309–20.
- [24] Gupta S, Ray A. Symbolic dynamic filtering for data-driven pattern recognition. In: Zoeller EA, editor. *Pattern recognition: theory and application*. Hauppauge, NY, USA: Nova Science Publisher; 2007 [chapter 2].
- [25] Buhl M, Kennel M. Statistically relaxing to generating partitions for observed time-series data. *Phys Rev E* 2005;71(4):046213.
- [26] Mallat S. *A wavelet tour of signal processing*. 2nd ed. San Diego, CA, USA: Academic Press; 1998.
- [27] Cover TM, Thomas JA. *Elements of information theory*. New York, NY, USA: Wiley; 1991.
- [28] Bapat RB, Raghavan TES. *Nonnegative matrices and applications*. Cambridge, UK: Cambridge University Press; 1997.
- [29] Keller EE. Real time sensing of fatigue crack damage for information-based decision and control, PhD thesis, Department of Mechanical Engineering, Pennsylvania State University, State College, PA; 2001.
- [30] Nagy P. Fatigue damage assessment by nonlinear ultrasonic materials characterization. *Ultrasonics* 1998;36:375–81.
- [31] Cantrell J, Yost W. Nonlinear ultrasonic characterization of fatigue microstructures. *Int J Fatigue* 2001;23:487–90.
- [32] Rose J. *Ultrasonic waves in solid media*. Cambridge, UK: Cambridge University Press; 2004.
- [33] Suresh S. *Fatigue of materials*. Cambridge, UK: Cambridge University Press; 1998.
- [34] Gupta S, Ray A. Pattern identification using lattice spin systems: a thermodynamic formalism. *Appl Phys Lett* 2007;91(19):194105.
- [35] Gupta S, Ray A. Real-time fatigue life estimation in mechanical structures. *Meas Sci Technol* 2007;18:1947–57.